Available online at www.sciencedirect.com
ScienceDirect
Surface Science 602 (2008) 436–442
SURFACE SCIENCE
www.elsevier.com/locate/susc

Cerium oxide layers on the Cu(1 1 1) surface: Substrate-mediated redox properties

R. Wrobel [1], Y. Suchorski *, S. Becker, H. Weiss

Chemisches Institut, Otto-von-Guericke-Universität Magdeburg, Universitätsplatz 2, D-39106 Magdeburg, Germany

Received 14 August 2007; accepted for publication 19 October 2007
Available online 5 November 2007

Abstract

Ceria submonolayers consisting of nanosized 2D islands on a Cu(1 1 1) surface have been prepared by oxidation of the nucleating Ce submonolayer (0.7 ML) and characterized using XPS and STM. The reducibility of the resulting well-defined CeO_{2-x}/Cu(1 1 1) model system of the "inverse supported catalyst" type was studied by XPS using CO as reducing agent. In order to investigate the contribution of the substrate in the redox process, the properties of a ceria submonolayer (0.7 ML) on Cu(1 1 1), of an optically dense layer of ceria (1.5 ML) on Cu(1 1 1) and of a ceria submonolayer (0.7 ML) on Pt(1 1 1) have been compared. The direct comparison reveals the (metal substrate mediated) spillover mechanism of the ceria reduction by CO in the present CeO_{2-x}/Me_{fcc}(1 1 1) model systems.

Keywords: X-ray photoelectron spectroscopy; Redox properties; Metal-oxide interface; Carbon monoxide; Oxygen; Cerium oxide; Platinum; Copper; Supported catalyst

1. Introduction

Ceria-based supported catalysts are widely used for hydrogenation and oxidation reactions [1–3], for synthesis of alcohols [4] and for automotive exhaust gas conversion [5], where the unique ability of ceria to store and to release oxygen during the oxidation and reduction stages is of particular interest [2,6]. Although the redox changes are important in most of the catalytic ceria applications, the atomistic understanding of the specific role of the cerium oxide, the catalytic metal component and the interfacial region between them in the complex redox mechanisms is, despite of great efforts, still incomplete.

Several important properties of oxide-based supported catalysts could be revealed by studying the well-defined model catalysts. Modern methods of nanofabrication such as electron-beam [7,8] or colloidal [9] lithography allows a controlled preparation of such well-defined model systems in the form of ordered arrays of small metal particles on a planar oxidic support. As an alternative approach, "inverse supported catalysts" where oxide islands cover the metal catalyst surface may also contribute to our understanding of processes at the metal-oxide interface during an ongoing reaction [10].

Recently, we have succeeded in assembling a well-defined CeO_{2-x}/Pt(1 1 1) "inverse supported catalyst" model system by exploiting the indirect interaction of Ce adatoms for the initial nucleation of Ce 2D nanostructures. A subsequent oxidation of the nucleating Ce submonolayer upon warming-up to room temperature at low oxygen pressure creates a system consisting of CeO_{2-x} islands more or less uniformly distributed on the Pt(1 1 1) surface. The CeO_{2-x} redox properties of this model catalytic system were studied by in situ XPS during the ongoing CO oxidation reaction, whereas a pronounced redox behaviour that directly related to the hysteresis cycle of the reaction was observed [11].

In the present work we apply a similar approach to the creation of a CeO_{2-x}/Cu(1 1 1) model system in order to compare the redox properties of CeO_{2-x}/Cu(1 1 1) and

* Corresponding author. Tel.: +49 391 67 18 824; fax: +49 3916711396.
E-mail address: Yuri.Suchorski@vst.uni-magdeburg.de (Y. Suchorski).
[1] On leave from Technical University of Szczecin, Szczecin, Poland.

0039-6028/$ - see front matter © 2007 Elsevier B.V. All rights reserved.
doi:10.1016/j.susc.2007.10.044

CeO_{2-x}/Pt(1 1 1). The idea is to vary the electronic structure of the metal component in the CeO_{2-x}/Me system while keeping the surface atomic geometry and the state of the cerium oxide component similar. This might shed light on the role of the metal substrate and of the metal-oxide interface in the reduction and re-oxidation of CeO_{2-x} nanoformations.

The method of choice for monitoring variations of the oxidation state of a metal oxide is still X-ray photoelectron spectroscopy (XPS). It encounters, however, significant difficulties in the case of cerium CeO_{2-x} suboxides. Although the ground state of Ce in CeO_2 is $4f^0$, a hybridization of the oxygen 2p valence band and 4f orbitals induces an f-character of the valence band states. In turn, in Ce_2O_3 Ce is in a $4f^1$ state, since the potential hybridization energy is significantly lower than the energy necessary for an electron transfer from the oxygen 2p band to the 4f state. The extraction of a core electron in a photoionization process results, via creation of a corresponding core hole, in a severe reorganization of the valence electrons, where the hybridization of the oxygen 2p valence band and 4f orbitals will take place, both for CeO_2 and Ce_2O_3. This results in the presence of three structures in the Ce $3d_{5/2}$ lines for CeO_2 and of two structures for Ce_2O_3, correspondingly [12]. Taking into account the spin-orbit splitting, the XP spectrum for the whole Ce 3d region of a CeO_{2-x} sample contains therefore ten peaks. This means a total of 30 parameters, namely the peak positions, the relative peak intensities and the FWHMs for each of the peaks need to be considered.

The deconvolution of these complicated XP spectra is especially difficult in the case of low-level Ce 3d signal, as e.g. from CeO_{2-x} submonolayers, since the possibility to increase the intensity of the X-ray excitation or the exposition time is limited due to photoreduction effects [13,14]. In the present study we solved this problem by calibration of the Ce 3d peak positions using a well-defined CeO_{2-x} multilayer with known Ce oxidation state deposited on the same Cu(1 1 1) sample which was used later as substrate for the CeO_{2-x} nanoformations.

2. Experimental

Experiments were performed in an ultrahigh vacuum (UHV) multipurpose surface analysis system operating at base pressures $\leqslant 10^{-10}$ mbar. In the present study X-ray photoelectron spectroscopy (XPS; SPECS, Phoibos-150), scanning tunnelling microscopy (STM; Omicron, VT-AFM/STM), as well as combined Auger electron spectroscopy and low energy electron diffraction (AES, LEED; SPECS, ErLEED 150) have been used.

The Cu(1 1 1) single crystal sample was a 1 mm thick disk of 10 mm in diameter. The standard surface cleaning procedure consisted of 1.5 keV argon ion sputtering at room temperature followed by annealing in UHV at 970 K. After several repetitions of the above procedure no contamination could be detected by XPS and a sharp hexagonal LEED pattern with low background was observed (Fig. 1a). The corresponding STM images show flat 20–50 nm wide terraces (Fig. 1b) separated by 0.21 nm high steps (Fig. 1c).

The Pt(1 1 1) crystal used for the comparison measurements was also a 1 mm thick disk of 10 mm in diameter, and was cleaned by 1.5 keV Ar^+ ion sputtering followed by annealing in oxygen (6×10^{-8} mbar) at 750 K and flashing in UHV to 1050 K.

The cerium overlayers were deposited using a commercial UHV-Evaporator (Focus EFM 3, Omicron) and the surface density of deposited cerium adatoms was estimated by AES analysis, following the procedure described in Ref. [15].

The XP spectra (pass energy 10 eV, step size 0.1–0.2 eV) were recorded with a 150 mm hemispherical energy analyzer using a Mg-K_α (1253.64 eV) X-ray source for the excitation. For studying the redox properties of the ceria overlayers the differentially pumped UHV chambers were run as constant flow reactors by admitting the reactive gases (CO, O_2) via leak valves from constant pressure reservoirs under mass-spectrometric control (MKS Instruments, VacCheck).

3. Results and discussion

The main goal of the present study was to study the redox behaviour of ceria nanoformations on Cu(1 1 1) surface in order to compare it directly with that on the Pt(1 1 1) surface and to reveal in this way details of the redox mechanism and the role of the metallic substrate in the redox process.

As already mentioned in the Introduction, the determination of the Ce oxidation state in submonolayers CeO_{2-x} is still a difficult task because of the difficulties in choosing proper values for the 30 parameters in the Ce 3d spectra at low XP signal intensity (low Ce density). In the case of low XP amplitude it appeared to be helpful to use a well-defined uniform reference sample that provides an XP signal level sufficient for a unambiguous oxidation state determination via the relation of oxygen/cerium peaks. A direct comparison with the results of the peak deconvolution allows then the proper positioning of each of the particular Ce^{3+} and Ce^{4+} contributions. The obtained parameters (peak positions, FWHMs and relative contributions) can then be used for deconvolution of the low-signal spectra from a non-uniform, heterogeneous adsorption system, where adsorbates such as oxygen or CO might also affect the results of evaluation. In our previous work Ar^+-sputtered CeO_2 samples (oxygen atoms in the surface region are preferentially released under the impact of Ar^+, providing partially reduced ceria) were successfully used as reference [8]. In the present study, we use a partially oxidized Ce multilayer on Cu(1 1 1) which is successively oxidized to CeO_2 in an oxygen atmosphere. An example of the evolution of the particular peaks is seen in Fig. 1 where the Ce 3d spectrum of partially oxidized CeO_{2-x} (Fig. 1e,

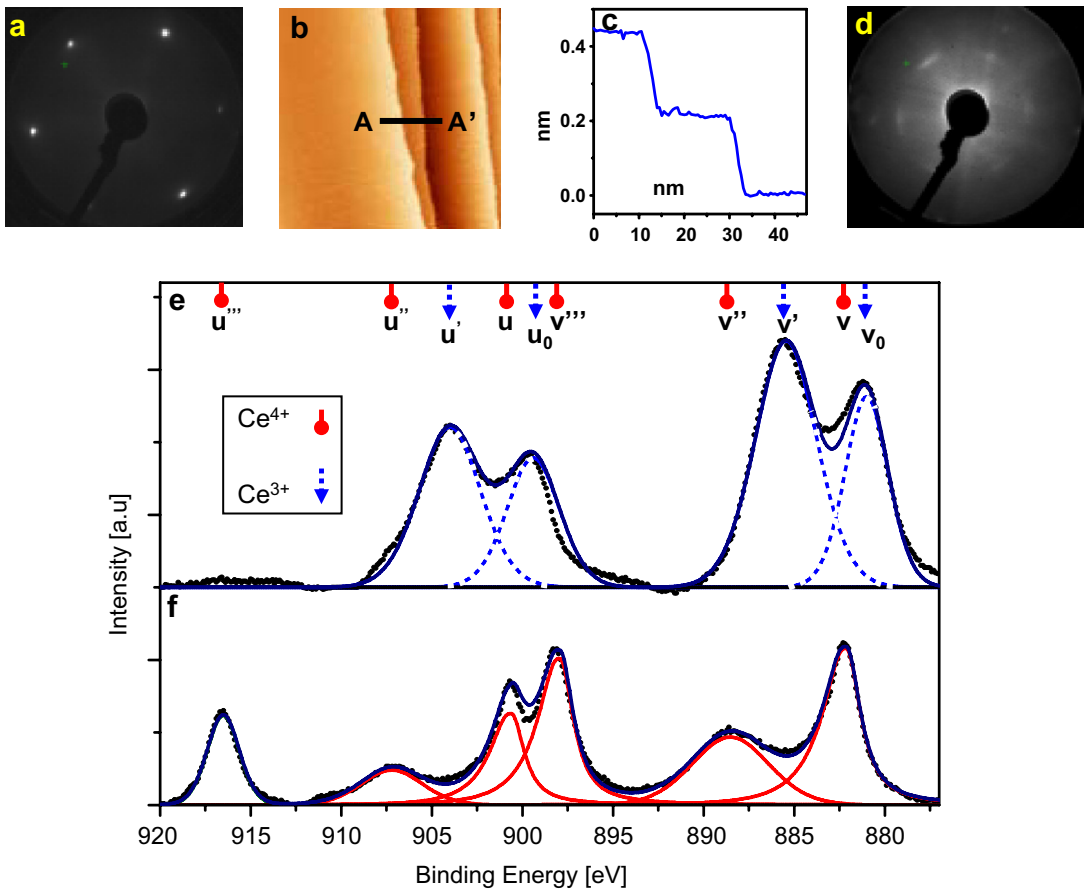

Fig. 1. Epitaxial ceria multilayer on Cu(1 1 1): (a) LEED pattern of the clean Cu (1 1 1) single crystal surface obtained at an electron energy of 98 eV. (b) STM image of the same surface (200 x 200 nm, $U_{bias} = 0.67$ V, $I_{tip} = -0.22$ nA). (c) A typical atomic step profile taken along A–A' in (b). (d) LEED pattern of an epitaxial ceria multilayer (12 ML) on Cu(1 1 1), electron energy 98 eV. The corresponding XP spectrum is shown in (f). (e) high-resolution Ce 3d XP spectrum (and its deconvolution) of a partially oxidized Ce layer (CeO_{2-x}, $x = 0.5$, 12 ML). The positions of particular peaks $u^{(index)}$ and $v^{(index)}$ attributable to Ce^{4+} and Ce^{3+} used for the spectra deconvolution are also shown. (f) The same, but for the fully oxidized Ce layer (>95% of Ce^{4+} contribution).

$x = 0.5$) is shown together with a spectrum obtained from the same sample but after completed oxidation to CeO_2 (Fig. 1f). The deconvolution of the obtained Ce 3d spectra using the different Gaussian-like peaks $u^{(index)}$ and $v^{(index)}$ (for the assignment of the individual peaks see Ref. [16]) allows to adjust the exact positions of the fitting components. Fig. 1d shows a corresponding LEED picture evidencing an epitaxial structure of the ceria multilayer.

After the calibration of the Ce 3d XP spectra, the ceria multilayer was sputtered off and the crystal was cleaned using the above described procedure. Then a Ce layer of 1.5 ML was deposited on the Cu(1 1 1) surface. To suppress the Ce–Cu alloy formation in present experiments, the Cu sample was cooled to 125 K during the Ce deposition. Immediately after deposition of Ce oxygen was introduced at 10^{-6} mbar and the sample was simultaneously heated from 125 to 723 K in order to achieve the partial oxidation of the Ce layer at the lowest possible temperature. After its entire oxidation at 723 K ($p_{O_2} = 10^{-6}$ mbar, 600 L, Fig. 2a) the resulting ceria layer (cerium oxidation state 3.9) was exposed to CO at 423 K and at $p_{CO} = 7 \times 10^{-5}$ mbar, at increasing CO exposures (up to $\sim 10^6$ L), and Ce oxidation state was XPS-monitored, but no reduction of ceria was observed under these conditions, neither at zero detection angle (electrons emitted normal to the surface, Fig. 2b), nor at higher detection angles. Subsequent exposure at 523 K (at $p_{CO} = 7 \times 10^{-5}$ mbar, $\sim 10^6$ L) showed still no reduction at zero detection angle, but revealed small changes at a detection angle of 50° that corresponds to a smaller information depth (Fig. 2c and d). These hardly detectable changes are not sufficient for a quantitative estimation of the Ce^{3+} contribution and should be treated rather as an experimental indication of the initiating reduction process at extremely large exposures and elevated temperatures. The appearance of the reduced cerium species at increasing detection angles indicates that in the present case the changes are caused rather by the reduction process in the CeO_x surface layer than by Ce-Me alloy formation beneath (at the CeO_x–Me interface) as was reported for thermal treating of ceria layers in UHV on Rh(1 1 1) [17]. We note that studies by Pfau and Schierbaum on "thick" ceria layers (10–40 nm, [16]) have also shown an extremely

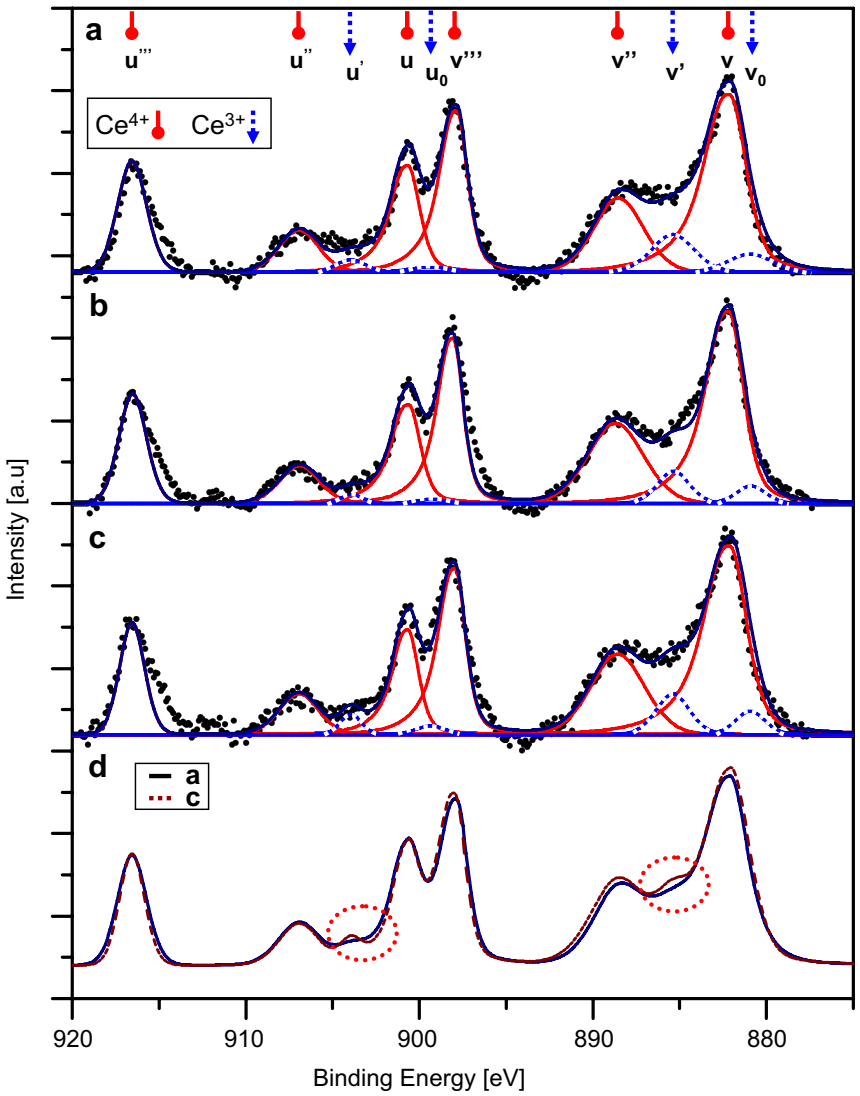

Fig. 2. Redox properties of an optically dense ceria layer (1.5 ML) on Cu(1 1 1): (a) Ce 3d XP spectrum (and its deconvolution) of a Ce layer oxidized at 723 K ($(p_{O_2} = 10^{-6}$ mbar, 600 L). (b) The same after exposure to CO at 423 K at $p_{CO} = 7 \times 10^{-5}$ mbar ($\sim 10^6$ L). (c) The same after subsequent reduction at 523 K at $p_{CO} = 7 \times 10^{-5}$ mbar ($\sim 10^6$ L), but taken at a detection angle of 50°. (d) Direct comparison of the normalized spectra (a) vs (c). The small changes indicating the only initial stages of the reduction process are marked by dotted circles.

low reducibility of ceria layers: an exposition to 10 bar of H_2 at 573 K was necessary to observe changes comparable to those shown in Fig. 2d. Thus it can be concluded that the direct interaction of the reducing atmosphere, CO in the present case, with the surface of an optically dense (as evidenced by STM measurements) CeO_2 film ($\Theta > 1$) leads, if at all, to a hardly observable reduction of its topmost surface layer even at very high exposures and elevated temperatures.

The possible role of the substrate in the reduction process can be studied by creating a ceria submonolayer where the Cu(1 1 1) substrate is also exposed to the reducing agent. For this purpose, a ceria submonolayer covering ca. 70% of the substrate surface was prepared using the same procedure as previously for the "thick" layer and controlling the Ce coverage by AES as described in Ref. [11]. A nanoscale visualisation of the created CeO_{2-x}/Cu(1 1 1) system by STM (see inset in Fig. 3b) confirms the coverage value and shows a similar topography as the recently studied CeO_{2-x}/Pt(1 1 1) inverse catalyst model system: 2D islands of 5–10 nm size are distributed stochastically over the surface [11]. The corresponding XP spectrum is shown in Fig. 3a together with the spectrum of the "thick" ceria film (12 ML). The comparison of the Ce 3d XP intensities of the CeO_{2-x} submonolayer and the "thick" ceria film illustrates the difficulties in the deconvolution of the obtained "low intensity spectra". Nevertheless, by using the calibration data obtained for the epitaxial ceria multilayer, it was possible to deconvolute the Ce 3d spectra: the corresponding deconvolution of the "low signal" XP spectrum of the oxidized ceria submonolayer is shown in Fig. 3b and provides an initial oxidation state of cerium about 3.7. It seems to be the highest possible oxidation state achievable under present UHV

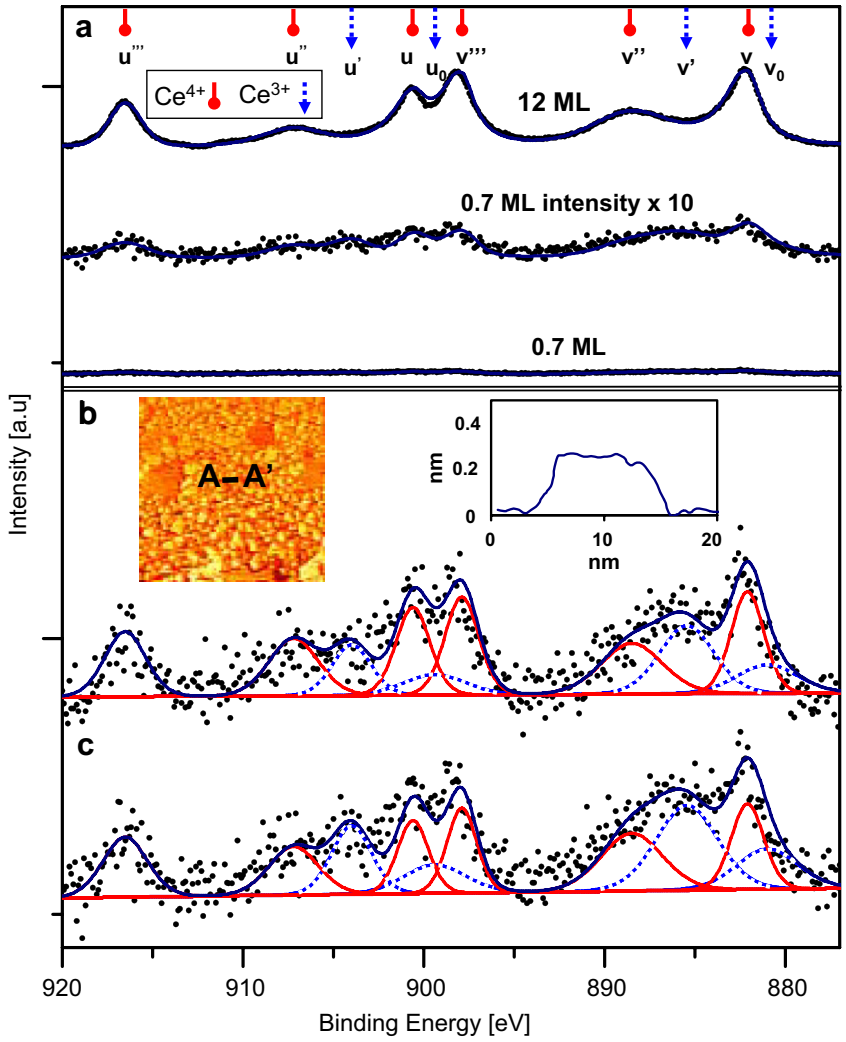

Fig. 3. Redox properties of a ceria submonolayer (0.7 ML) on Cu(1 1 1): (a) Comparison of the XP intensity for the oxidized Ce submonolayer (0.7 ML, lower curve) with that of a ceria multilayer (12 ML, upper curve) illustrating the difficulties in the deconvolution of the "low intensity spectra". The middle curve corresponds to the lower one (submonolayer) magnified by a factor of 10. (b) Deconvolution of the above Ce 3d XP spectrum for the oxidized Ce submonolayer. The insets show a corresponding STM image (234.5 x 234.5 nm, $U_{bias} = -0.55$ V, $I_{tip} = 0.26$ nA) and a typical 2D ceria island profile taken along A–A' (a marginal number of double-height islands was also observed). (c) The same as in (b), but after prolonged exposure to CO at 423 K ($p_{CO} = 7$ x 10^{-5} mbar, $\sim 10^6$ L). Ce^{4+} content is reduced from 71% to 64%. Absolute intensities of the Ce 3d signal and the signal-to-noise ratio in this figure are not directly comparable with those in Fig. 4 (ceria submonolayer on Pt) because of differing XPS adjustments and larger background pressure in the Cu case due to prolonged reduction attempts.

conditions, i.e. after the oxidation performed using same procedure as for 1.5 ML layer. The reason for this lies, in our opinion, in the interaction of Ce atoms (especially of those at island borders) in 2D islands with both, Cu- and O-atoms, whereas in thicker ceria layers only Ce atoms in the "bottom" layer are involved in such a "double" interaction.

As in the case of the 1.5 ML ceria film, the ceria submonolayer was consequently exposed to CO at 423 K and at $p_{CO} = 7 \times 10^{-5}$ mbar, at increasing CO exposures (up to $\sim 10^6$ L), and Ce oxidation state was XPS-monitored. In contrary to the dense ceria layer, the reduced CeO_{2-x} submonolayer shows a clearly detectable increase in its Ce^{3+} content from 29% to 36% (Fig. 3c). This result makes evident that the reducibility of the ceria submonolayer by CO as reducing agent is much higher than for the dense ceria layer on Cu(1 1 1). It is clear that the substrate may play a deciding role in this finding, namely, a spillover mechanism of the diffusive CO transport to the CeO_{2-x} nanoformations is conceivable.

This supposition can be verified by replacing the Cu(1 1 1) surface by another one of different CO adsorption activity. To avoid a possible effect of the atomic surface geometry, the (1 1 1) surface of another fcc metal would be preferable. Platinum is a suitable candidate, since it has a close lattice constant of $a_{Pt} = 0.39$ nm ($a_{Cu} = 0.36$ nm) but exhibits in the case of the (1 1 1) surface drastically different adsorption properties with respect to CO [18,19].

A ceria submonolayer (0.7 ML) was prepared on the Pt(1 1 1) surface using the same procedure as for the

Cu(1 1 1) surface and was exposed subsequently to CO at 423 K ($p_{CO} = 1.3x10^{-6}$ mbar, 300 L). The results are shown in Fig. 4: despite the much lower exposure to the reducing atmosphere (in comparison to the CeO_{2-x}/Cu(1 1 1) system) the average cerium oxidation state has already changed from 3.92 to 3.65 (Fig. 4a vs 4b). A subsequent exposition to CO under the same pressure and dosage but at a higher temperature of 523 K causes a further remarkable evolution of the Ce oxidation state from 3.65 to 3.43. No changes of the Ce oxidation state were observed in turn, when the present system was thermally treated in the same way in UHV. This excludes a meaningful contribution of the additional processes, such as e.g. thermal decomposition of ceria or Ce–Pt alloy formation in the increase of the Ce^{3+} fraction.

The spectra shown in Figs. 3 and 4 demonstrate a dramatic discrepancy in the reducibility of ceria submonolayers of the same coverage (0.7 ML) on two densely packed fcc (1 1 1) surfaces of closely related surface corrugation (Cu vs Pt). Since the direct interaction of CO with the ceria surface itself does not lead to an observable reduction in UHV conditions (see Fig. 2), the adsorption properties of both electronically differing metallic substrates must be responsible for such a striking difference. In the case of Cu(1 1 1) the relatively low binding energies of CO in the range of 35–38 kJ/mol for high coverages and of 44–50 kJ/mol for low coverages, correspondingly, [20,21], hinder the CO adsorption under UHV conditions at the given temperatures (>300 K): the "high-temperature" thermodesorption peak for CO on Cu(1 1 1) is found at 170 K [19]. This also inhibits e.g. effectively the CO oxidation reaction on Cu(1 1 1) in UHV, as was evidenced in demostrative PEEM experiments on the Cu-modified Pt(1 1 1) surface [22].

In turn, the much higher binding energies of CO on Pt(1 1 1), ranging from 92 kJ/mol [23] at high to 145 kJ/mol [24] at low coverages, respectively, coupled with a high

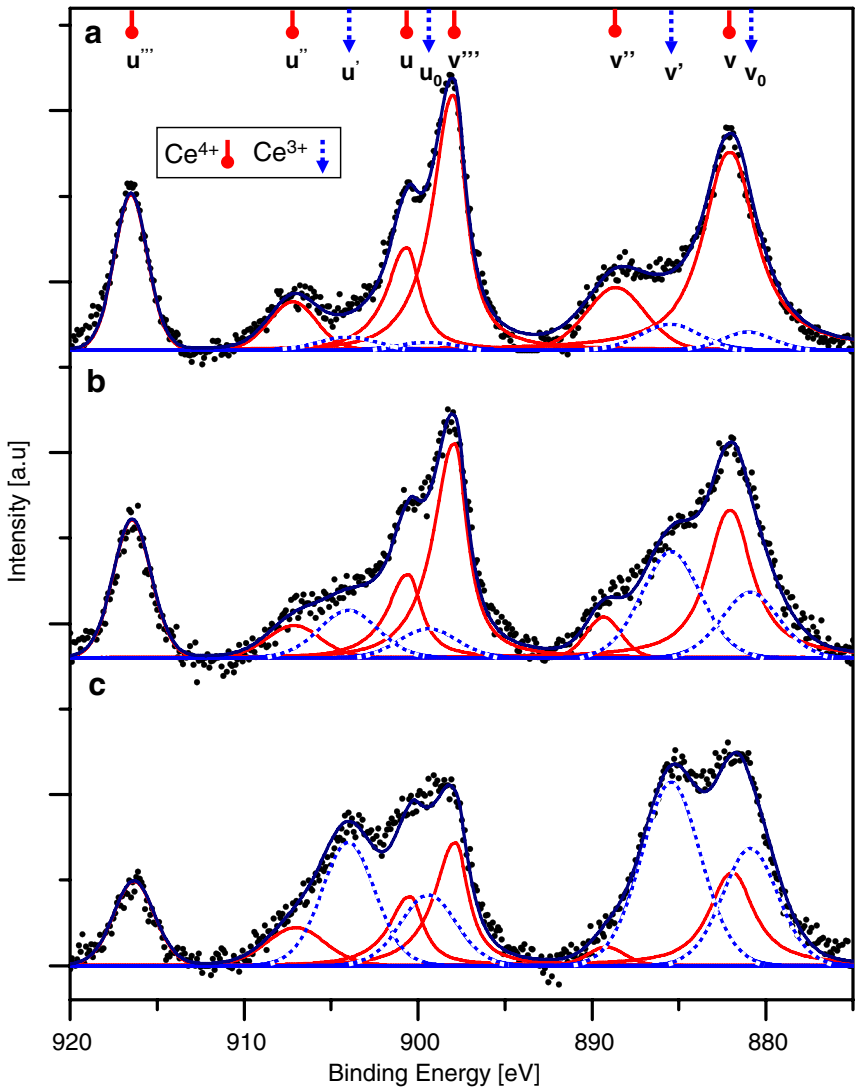

Fig. 4. Redox properties of a ceria submonolayer (0.7 ML) on Pt(1 1 1): (a) Ce 3d XP spectrum (and its deconvolution) of the oxidized Ce submonolayer (0.7 ML) on the Pt(1 1 1) surface. (b) The same after exposure to CO at 423 K ($p_{CO} = 1.3 \times 10^{-6}$ mbar, 300 L). The Ce^{4+} content is reduced from 92% to 68%. (c) The same, but after a further exposure to CO at 523 K ($p_{CO} = 1.3 \times 10^{-6}$ mbar, 300 L). The Ce^{4+} content is further reduced from 68% to 43%.

initial sticking coefficient (0.84 at 300 K, [25]) provide an effective uptake of CO even at elevated temperatures [26]. In addition, highly mobile surface CO species emerge at higher CO coverages [27]. The presence of a mobile CO layer is the difference between the CeO_{2x}/Pt(1 1 1) and CeO_{2-x}/Cu(1 1 1) systems in our experiments in which ceria on Pt(1 1 1) turned out to be much easier reducible than on Cu(1 1 1). This allows us to postulate a substrate-mediated spillover mechanism for the ceria reduction by CO in the present CeO_{2-x}/Me(1 1 1) model systems. Although such a spillover mechanism (metallic particles activate gas molecules allowing them to diffuse to the oxide support substrate surface) has been suggested for the hydrogen species on ceria-supported Pt and Pd catalysts [28], and the principal possibility for the CO species to spillover from metal clusters to an oxide was mentioned e.g. for Pt/ZrO_2 catalysts [29], detailed studies on the CO spillover effect in redox processes have to our knowledge still been lacking.

In conclusion, we note that inverse supported model catalysts prepared on well-defined single crystal metal surfaces are more suited for studying direct (from metal to oxide) spillover effects than the systems consisting of metal clusters deposited on a planar oxide surface, since both the adsorption and diffusion properties of reducing agents such as CO or hydrogen are well-studied for the single crystal surfaces of most of the platinum group metals.

4. Summary

A well-defined CeO_{2-x}/Cu(1 1 1) model system of the "inverse supported catalyst" type has been fabricated by oxidizing nucleating Ce 2D islands on the Cu(1 1 1) surface, and the reducibility of the resulting submonolayer ceria film (coverage 0.7 ML) by CO was investigated with XPS. The obtained results demonstrate an essential role of the metallic substrate in the redox process: a direct comparison of the reducibility of the ceria submonolayer with that of an optically dense ceria film on Cu(1 1 1) allows to suggest a spillover mechanism of the CO supply from the metal surface towards the CeO_{2-x} islands. To prove this suggestion, the reducibility of a 0.7 ML CeO_{2-x}/Pt(1 1 1) model system has been studied under the same conditions. The comparison of the results obtained for both submonolayer systems, which differ significantly in the electronic properties of the metal substrate but have an almost identical surface geometry, confirms the substrate-mediated spillover mechanism for the ceria reduction by CO in the present CeO_{2-x}/Me_{fcc}(1 1 1) model systems. This demonstrates the suitability of the used type of inverse model catalysts prepared on well-defined single crystal metal surfaces for the investigation of direct (from metal to oxide) spillover effects.

Acknowledgement

R.W. acknowledges the support by EU contract HPRN-CT-2002-00191.

References

[1] A. Trovarelli, Catal. Rev.– Sci. Eng. 38 (1996) 439, and references therein.
[2] D. Duprez, C. Descorme, in: A. Trovarelli (Ed.), Catalysis by Ceria and Related Materials, Imperial College Press., 2002, p. 243.
[3] S. Chettibi, R. Wojcieszak, E.H. Boudjennad, J. Belloni, M.M. Bettahar, N. Keghouche, Catal. Today. 113 (2006) 157.
[4] C.R. Apesteguia, B. De Rites, S. Miseo, S. Soled, Catal. Lett. 44 (1997) 1.
[5] J. Kaspar, M. Graziani, P. Fornasiero, in: K.A. Gschneider, L. Eyring (Eds.), Handbook on Physics and Chemistry of Rare Earths, vol. 29, Elsevier Science B.V., 2000, p. 159, and references therein.
[6] V.P. Zhdanov, B. Kasemo, Appl. Surf. Sci. 135 (1998) 297.
[7] G.A. Somorjai, Appl. Surf. Sci. 121/122 (1997) 1.
[8] A. Avoyan, G. Rupprechter, A.S. Eppler, G.A. Somorjai, Top.Catal. 10 (2000) 107.
[9] L. Österlund, S. Kielbassa, C. Werdinius, B. Kasemo, J. Catal. 215 (2003) 94.
[10] K. Hayek, M. Fuchs, B. Klötzer, W. Reichl, G. Rupprechter, Top. Catal. 13 (2000) 55.
[11] Y. Suchorski, R. Wrobel, S. Becker, B. Strzelczyk, W. Drachsel, H. Weiss, Surf. Sci. 601 (2007) 4843.
[12] M. Romeo, K. Bak, J. El Fallah, F. Le Normand, L. Hilaire, Surf. Interface Anal. 20 (1993) 508.
[13] Y. Suchorski, J. Gottfriedsen, R. Wrobel, B. Strzelczyk, H. Weiss, Solid State Phenom. 128 (2007) 115.
[14] S.P. Chenakin, R. Prada Silvy, N. Kruse, Catal. Lett. 102 (2005) 39.
[15] E. Napetschnig, M. Schmid, P. Varga, Surf. Sci. 556 (2004) 1.
[16] A. Pfau, K.D. Schierbaum, Surf. Sci. 321 (1994) 71.
[17] S. Eck, C. Castellarin-Cudia, S. Surnev, M.G. Ramsey, F.P. Netzer, Surf. Sci. 520 (2002) 173.
[18] R.J. Gorte, L.D. Schmidt, Surf. Sci. 111 (1981) 260.
[19] W. Kirstein, B. Krüger, F. Thieme, Surf. Sci. 170 (1986) 505.
[20] P. Hollins, J. Pritchard, Surf. Sci. 89 (1979) 486.
[21] J. Kessler, F. Thieme, Surf. Sci. 67 (1977) 405.
[22] R.E.R. Colen, M. Kolodziejczyk, B. Delmon, J.H. Block, Surf. Sci. 412/413 (1998) 447.
[23] G. Ertl, M. Neumann, K.M. Streit, Surf. Sci. 64 (1977) 393.
[24] H. Steininger, S. Lehwald, H. Ibach, Surf. Sci. 123 (1982) 264.
[25] C.T. Campbell, G. Ertl, H. Kuipers, J. Segner, Surf. Sci. 107 (1981) 207.
[26] P.R. Norton, J.W. Goodale, E.B. Selkirk, Surf. Sci. 83 (1979) 189.
[27] Y. Suchorski, Ultramicroscopy 73 (1998) 139, and references therein.
[28] A. Norman, V. Perrichon, A. Bensaddik, S. Lemaux, H. Bitter, D. Koningsberger, Top. Catal. 16/17 (2001) 363.
[29] J.J. Daniels, A.R. Arther, B.L. Lee, S.M. Stagg-Williams, Catal. Lett. 103 (2005) 169.